

Physical–chemical characterization of metal hydroxides sludge waste obtained from electrocoagulation processes and its application as adsorbent for organic pollutants removal in aqueous solution

Celestino García-Gómez^a, Juan Antonio Vidales-Contreras^a, Julia Mariana Márquez-Reyes^a, Arquímedes Cruz-López^b, Santiago Iván Suárez-Vázquez^{b,*}

^aUniversidad Autónoma de Nuevo León, Facultad de Agronomía, Francisco Villa S/N, C.P. 66050 General Escobedo, Nuevo León, México, Tel. +52+8183294000 Ext. 7256; emails: celestino.garciagm@uanl.edu.mx (C. García-Gómez), juan.vidalescn@uanl.edu.mx (J.A. Vidales-Contreras), jmmarquez23@gmail.com (J.M. Márquez-Reyes)

^bUniversidad Autónoma de Nuevo León, Facultad de Ingeniería Civil, Cd. Universitaria, Av. Universidad S/N, San Nicolás de los Garza 66455, Nuevo León, México, emails: santiago.suarezvz@uanl.edu.mx, ssuarezvazquez@gmail.com (S.I. Suárez-Vázquez), cruz_lopeza@yahoo.com.mx (A. Cruz-López)

Received 18 September 2018; Accepted 11 March 2019

ABSTRACT

The present work aims at the reuse of metal hydroxide sludge generated by an electrocoagulation process. Its application in the adsorption of pollutants present in aqueous medium is also studied using Congo red as a molecule model and batch reactors. The characterization results demonstrate the presence of the boehmite phase with acceptable textural properties as adsorbent and high stability under different pH conditions. During the adsorption tests, it was shown that both, the pH and the initial concentration, produces a negative influence in the percentage of Congo red retention attributed to the electrostatic repulsion between OH⁻ and Congo red at high pH values on one hand and the absence of active sites at high concentration levels on the other hand. On the contrary, the increase in Congo red adsorption was proportional to the temperature associated with the thermodynamic characteristics of the adsorption process that are also presented in this work. The performance of the adsorption followed a second-order kinetics that indicates that adsorption followed a cation exchange process between the adsorbent and adsorbate; besides that different models were applied (Freundlich, Langmuir and Temkin), the Freundlich model described the better adsorption process of Congo red indicating adsorption on a heterogeneous surface and multilayer formation.

Keywords: Adsorption; Organic dye; Metal hydroxide sludge; Batch; Physical–chemical characterization

1. Introduction

The Congo red (CR, sodium salt of benzidinediazo-bis-1-naphthylamine-4-sulfonic acid) is a water soluble anionic diazo dye with beneficial aspects such as the detection of amyloidosis, however is also characterized by being carcinogenic and high toxicity [1]. It is widely used in different industries such as textiles, plastics, rubbers, printing,

leather, paper, pharmaceutical, food and cosmetics, where a large amount of this dye is released into the aquatic system causing serious pollution problems and generating a major challenge for the agencies of environmental protection [1]. This challenge is increasing due to the high chemical recalcitrance of the CR generated by its aromatic structure with rings of benzene and naphthalene, which gives it a high optical, thermal and physicochemical stability making it

* Corresponding author.

difficult to achieve the degradation of the CR by conventional methods [2]. Due to the above discussion, the discharge of industrial effluents containing this type of dyes influences the natural appearance of the rivers. It is estimated that between 10% and 15% of the CR used in some applications previously mentioned is released annually in water bodies [3,4]. This action produces a negative impact in aquatic life, due to the carcinogenic and mutagenic effects of the CR as well as the interference of sunlight. The later impact is related with a decrease of photosynthesis and causes an oxygen deficiency in the receiving water bodies [5,6]. Therefore, there is a need to design efficient and low-cost methods for the elimination of CR from aqueous effluents [7].

Various physical, chemical and biological methods such as adsorption using organic waste [8] or even graphene composites [8], chemical reduction [1], bioremoval with microalgae [9], electrochemical [10], cavitation [11], Fenton [12], photocatalytic [13], among others, have been widely used in the elimination of CR of residual effluents, but their effectiveness or economic advantage are factors that are still debated today. In this sense, adsorption is considered a promising technique with wide advantages because it is economical, with high performance and easy operation. Recent research focuses on the use of low-cost or natural adsorbents and the reuse of different agricultural or industrial residues [14–16], in this sense electrocoagulated metal hydroxide sludge (EMHS) is a candidate, which is obtained from an electrocoagulation (EC) process where aluminum or iron electrodes releasing hydroxides of these metals oxidize [17,18]. These materials are considered waste that can cause environmental and public health impacts if not managed properly. However, a practical application or reuse that can be granted to the EMHS is in the elimination of effluent dyes by electrostatic attraction or surface complexation as has been reported in recent years for different types of dyes [19,20] what becomes the motivation of this investigation. The implementation of an adsorption process requires a study of the adsorption equilibrium, kinetics, speed limiting steps and, thermodynamics, which is possible to be obtained from batch systems. The objective of this work is the complete characterization and evaluation of EMHS in its reuse as an adsorbent material evaluating the capacity of removal of contaminants present in aqueous medium. To do this, the CR dye was used as a molecule model and the adsorption tests were carried out in batch reactors. Within the adsorption studies, the effect of the process parameters such as pH, temperature, CR concentration, contact time, in addition to kinetics, isotherms and thermodynamics, were evaluated; and the relationship among adsorption capacities was established with the physicochemical characterization of the adsorbent.

2. Materials and methods

2.1. Adsorbent material

The adsorbent used in this study was obtained from a pilot EC plant using aluminum electrodes. The waste sludge obtained after EC was clarified, sedimented, centrifuged, dried, crushed and finally sieved with a mesh 35–40 (geometric diameter of 0.4018 mm). The material obtained

from this process was subsequently used for the adsorption experiments.

2.2. CR Solutions

Stock solution of Congo Red (molecular weight = 696.665 g mol⁻¹, molecular formula = C₃₂H₂₂N₆Na₂O₆S₂) (dye content ≥ 85% Sigma-Aldrich Inc., USA) was prepared by dissolving 1 g of CR powder in 1 L of distilled water. Subsequent dilutions of CR were made to obtain the desired initial concentration. Prior to the addition of EMHS, the initial pH of the experimental solution was adjusted to the desired conditions with the appropriate amounts of 0.1 M HCl or 0.1 M NaOH. The concentration of CR in the sample was analyzed using a UV-Vis spectrophotometer (Genesys 10S, Thermo Fisher Scientific Inc., USA) at a maximum wavelength of 497.5 nm.

2.3. Characterization of the adsorbent

The identification of the phases present in the adsorbent material was carried out by means of the X-ray diffraction (XRD) technique using an Empyrean Malvern Panalytical Ltd., (The Netherlands). equipment equipped with radiation Cu K α ($\lambda = 1.5418 \text{ \AA}$). Additionally, the average crystallite size (d_s) was calculated using the Scherrer equation [21]:

$$d_s = \frac{k \lambda}{\beta \cos \theta} \quad (1)$$

where d_s corresponds to the average crystallite size, k is the constant of Scherrer (0.89), λ corresponds to the wavelength of the X-rays (1.54 \AA), β is the broadening at half of the maximum intensity and θ is the Bragg's angle. On the other hand, the morphology of the particles as well as the elemental composition of the adsorbent material before and after the adsorption of CR were analyzed by the scanning electron microscopy technique and coupled with a detector for microanalysis by energy dispersion by X-rays (SEM-EDS) JEOL 6510 LV, JEOL (Japan).

The textural properties of the adsorbent were characterized by the N₂ physisorption technique using an Autosorb 3B device Quantachrome Instruments, USA. Additionally, the specific surface area was calculated using the Brunauer-Emmett-Teller (BET) method. Finally, the surface characterization was carried out by means of the Fourier transform infrared spectrometry technique coupled to a total attenuated reflectance device (ATR-FTIR) in the range of 630 cm⁻¹ up to 4,000 cm⁻¹ at a resolution of 4 cm⁻¹ using a Prestige 21 Shimadzu Co. (Japan). To perform the analysis, the samples were mixed with KBr in a 1:100 ratio and pressed to form a thin circular capsule.

2.4. Adsorption tests in batch reactors

The batch adsorption experiments were carried out in triplicate using a traditional bottle point method with which the effect of different reaction parameters was evaluated on the adsorption efficiency of CR, as the pH of the solution (2–12), temperature (303–323 K), initial concentration (25–500 mg L⁻¹) and the contact time (1–48 h). For this,

multiple experiments were carried out in 250 mL flasks, adding 100 mL of a CR solution with a known concentration and adjusting the pH as mentioned above. Subsequently, 1 g of adsorbent material was added and the flasks containing the reaction medium were sealed. The adsorption tests were carried out on a thermoregulated stirrer at a speed of 150 rpm at a pre-set temperature. At the end of the experiments, the samples were sedimented and no adsorption was observed in the glass walls of the flask. Finally, the concentration of CR maintained in the supernatant was analyzed using a UV–Vis spectrophotometer (Genesys 10 S, Thermo Fisher Scientific, USA) at a maximum wavelength $\lambda_{\max} = 497.5$ nm to determine the dye concentrations. The amount of dye adsorbed by the adsorbent was calculated by the following equation:

$$q_e = \frac{V(C_0 - C_e)}{m} \quad (2)$$

where q_e is the amount of dye in equilibrium (mg g^{-1}), V is volume of the dye solution (L), C_0 is the final concentration of dye in equilibrium after adsorption and m is the dry weight of the adsorbent (g).

3. Results and discussion

3.1. Characterization of EMHS

3.1.1. XRD analysis

Fig. 1 shows the X-ray diffractograms obtained before and after the CR adsorption tests carried out in batch at different pH values. It is possible to observe the presence of characteristic signals of boehmite, $\text{AlO}(\text{OH})$, according to the International Center for Diffraction Data, ICDD 01-074-2897 card with orthorhombic structure. This phase preserves independently of the pH value, confirming a good stability of the adsorbent at different acidic conditions. However, an additional signal observes in 26.63° in 2θ after the adsorption tests, which is possible due to the presence of CR retained on the surface of the adsorbent [22]. However, due to the

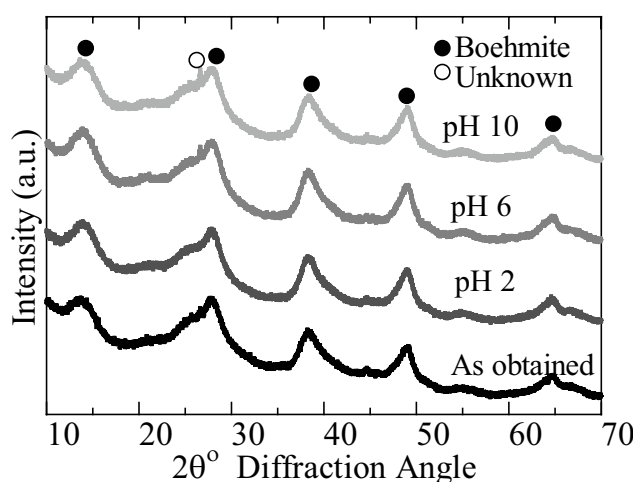


Fig. 1. X-ray diffraction of the adsorbent material before and after the adsorption tests at different pH.

low intensity and appearance as a narrow shoulder, it is difficult to confirm this statement for this reason, it is marked as unknown signal, but this peak does not appear in adsorbents treated at pH 2 neither in fresh sample but increases in intensity as function of the pH values from pH 6. From the diffractograms obtained in Fig. 1 the crystallite sizes of the adsorbent material were calculated using the peak signal (020) located at 14.421 in 2θ as previously reported [21]. The results show that the variation in pH does not perform a substantial effect on crystallite size since it remained in the range of 3.3–3.8 nm.

3.1.2. ATR-FTIR analysis

In Fig. 2 the ATR-FTIR spectra of the adsorbent materials are presented before and after the adsorption tests carried out at different pH values. In these spectra a wide peak is observed above $3,000 \text{ cm}^{-1}$ ($3,200\text{--}3,600 \text{ cm}^{-1}$) and a very weak peak at $2,050 \text{ cm}^{-1}$ are observed attributed to the vibrations by tension and flexion of the OH and a combination band with the water, respectively [23,24]. Within the width of this peak is identified the point of greatest adsorption located at $3,311 \text{ cm}^{-1}$ which, associated with the shoulder at $1,064 \text{ cm}^{-1}$, corresponds to the vibrational modes of stress and deformation of the OH, respectively, present in the boehmite [23,24], confirming the presence of this phase and its good stability at different pH values. Those adsorbent materials that were used for the adsorption of CR present a greater width of the peaks located between $3,200$ and $3,600 \text{ cm}^{-1}$, which may be due to the presence of NH_2 groups coming from the CR adsorbed on the surface of the adsorbent [24,25]. This figure also presents a remarkable peak at 954 cm^{-1} and ends with signals below 630 cm^{-1} , the first peak does not correspond to any link present in the boehmite phase or CR, however, this characteristic peak has been reported in attributed signals to the Si–OH bond [24,26]. The presence of Si may be due to the quality of the water used in the EC process from the generation of the adsorbent material. Finally, those signals below 630 cm^{-1} correspond as a part of the Al–O bonds present in the boehmite [24].

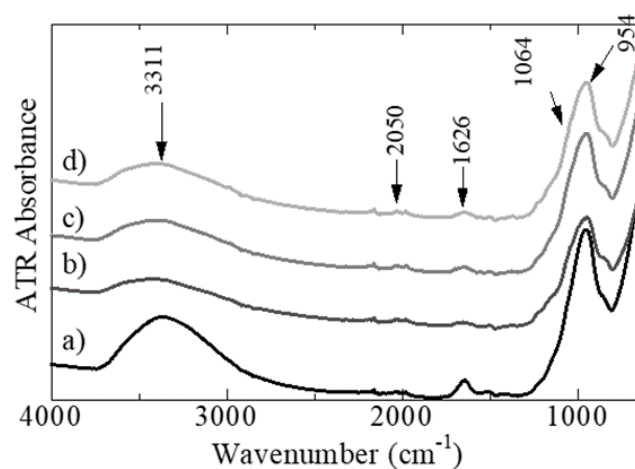


Fig. 2. ATR-FTIR of the adsorbent materials used in this work before and after the adsorption tests at different pH (a) before the adsorption, (b) pH 2, (c) pH 6 and (d) pH 10.

3.1.3. Textural analysis

In Fig. 3 the textural properties of the adsorbent material are presented. In particular Fig. 3a shows the adsorption–desorption isotherm of type IV [26] characteristic of a rough surface and which seems to reach the maximum saturation at relative pressures greater than 0.9. In addition, this type of isotherm is characteristic of mesoporous materials, which is evidenced in Fig. 3b where the pore size distribution is demonstrated, reaching the maximum peak around 74 Å pore diameter, which is within the range of this type of porosity. The hysteresis type H1 presented in this figure confirms both the formation of an isotherm type IV and the capillary condensation during filling of the mesoporous with a narrow pore size distribution as confirmed in Fig. 3b. This type of mesoporous materials are characteristic for presenting high surface area which is confirmed with the $302 \text{ m}^2 \text{ g}^{-1}$ value obtained for the boehmite used as adsorbent in this work and is very similar or even superior to other adsorbent materials reported previously [26,27]. According to these properties, this material is considered as an excellent candidate for adsorption of contaminants present in water bodies.

3.1.4. SEM analysis

To confirm both, the particle size and the presence of Si, SEM–EDS was carried out and the results are as shown in Fig. 4. Fig. 4a confirms the average particle size of 0.40 μm mentioned above for the adsorbent material in addition to the presence of heterogeneous morphology and rough surface. Fig. 4b demonstrates the roughness observed on the surface of the adsorbent that will contribute for the interaction with the CR. Additionally a decrease in the roughness of the surface attributed to the adsorption of CR as observed in Fig. 4c. Finally, the presence of Al and O mainly followed by 8.7 wt.% of Si is shown in Fig. 4d which coincides with the notable peak at 954 cm^{-1} observed in Fig. 2.

3.2. Batch adsorption tests

3.2.1. Effect of initial concentration

The adsorption of CR on EMHS was observed as a function of time until the amount removed from the dye became constant. Fig. 5a shows the behavior of the initial concentration at 50 mg L^{-1} as a function of the contact time during adsorption of CR at pH of 6.38 ± 0.23 and 298 K. Initial spontaneous adsorption occurred in the first 3 h, followed by a gradual increase until 26 h reaching $\approx 90\%$ removal, afterwards a slight increase in CR adsorption was observed, reaching up to $94.79\% \pm 0.18\%$ removal at 48 h. Therefore, from these results, the considered equilibrium time was 48 h for all subsequent experiments, regardless of the initial CR concentrations. The effect of the initial concentration of CR in the adsorption with EMHS was carried out by varying the concentrations of the dye (25, 50, 100, 200, 300 and 500 mg L^{-1}) at 298 K and contact time of 48 h. As seen in Fig. 5b, the percentage of CR removal by EMHS decreased by increasing the initial concentrations. For instance, at 25 mg L^{-1} with $94.39\% \pm 2.37\%$ removal, decreased up to $53.54\% \pm 6.05\%$ removal using 500 mg L^{-1} , which attributed to the lack of availability of active sites and pores for CR molecules in particles of the adsorbent material that occurs at high concentrations of contaminant [28].

3.2.2. Effect of pH

Fig. 5c shows the effect of pH (2–12) on the adsorption of CR using EMHS with a temperature of 298 K, initial concentration of 100 mg L^{-1} and contact time of 48 h. The adsorption capacity of the dye on EMHS showed a first decrease of $96.54\% \pm 1.65\%$ at $85.81\% \pm 4.95\%$ when the pH changed from 2 to 6. The percentage of adsorption remained constant in a pH range of 6–10, while increasing the pH to 12 a second decrease clearly occurred. Therefore, the maximum adsorption (data not shown) is located at pH below the point of zero charge (pH_{pzc}) attributed to the anionic

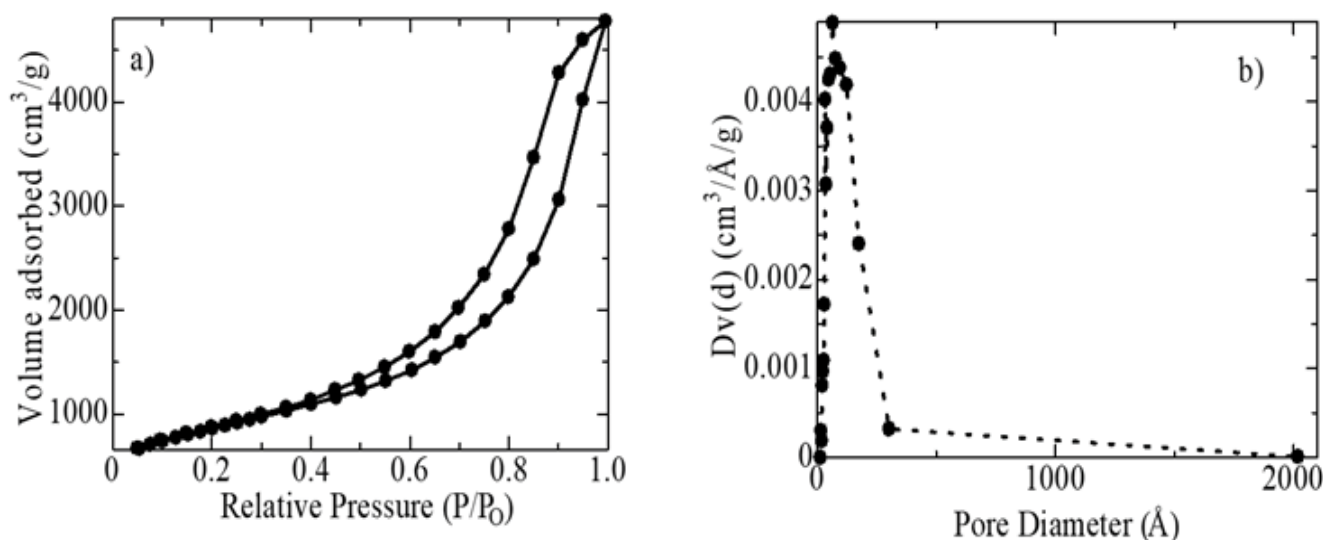


Fig. 3. Textural properties of the adsorbents used in this work. (a) Adsorption–desorption isotherm of N_2 and (b) pore size distribution.

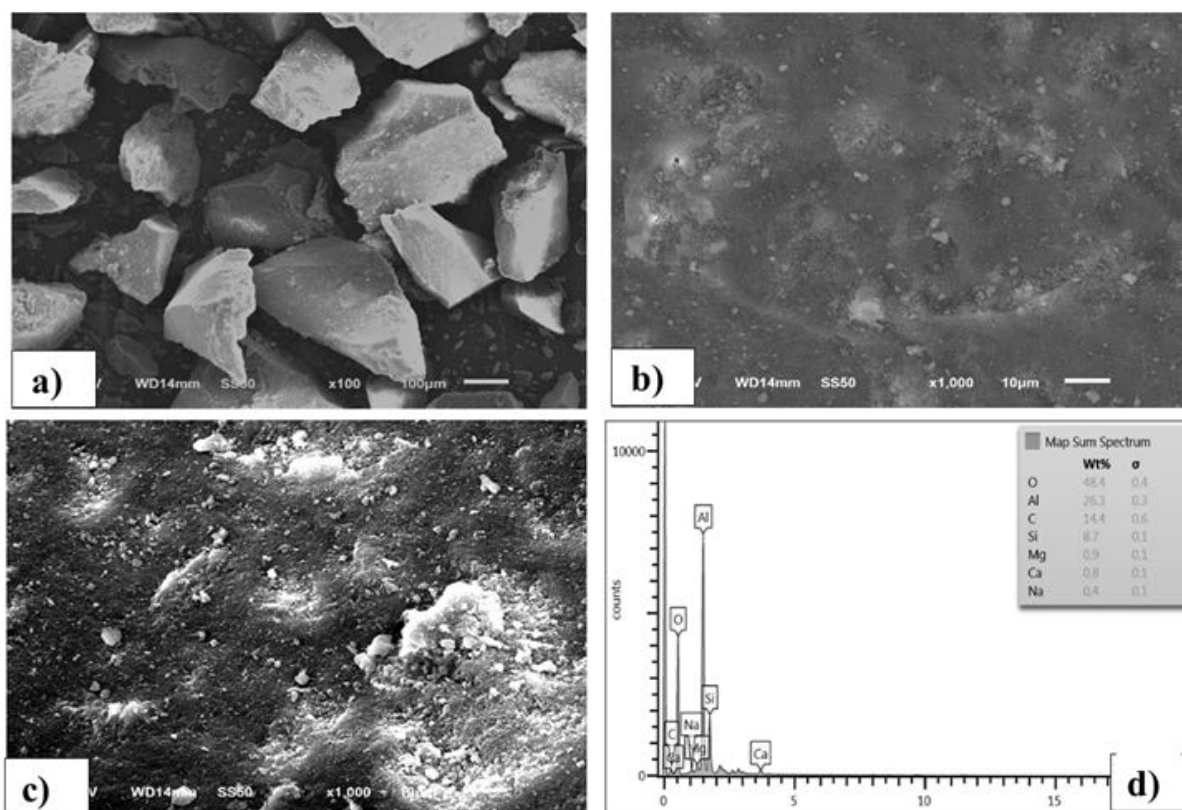


Fig. 4. SEM-EDS of EMHS: (a) particle size, (b) surface of the adsorbent before the adsorption tests, (c) surface of the adsorbent after the adsorption tests and (d) elemental analysis of the adsorbent.

adsorption favored by the increase in the positive charge density associated with the high concentration of H^+ ions at the adsorption sites and therefore, the higher electrostatic attraction between the solute and the adsorbent [29]. On the contrary, it is considered that, at pH above pH_{pzc} , high electrostatic repulsion between OH^- and the anionic dye gave rise to a relatively poor adsorption, mainly at pH higher than 10.

3.2.3. Effect of the temperature

Fig. 5d shows the percentage of CR removal as a function of the temperature of the solution during the CR adsorption process at neutral pH, initial concentration of 100 mg L^{-1} and contact time of 48 h. A growing trend in the percentage of dye removal occurred when the solution temperature changed from 303 to 323 K increasing from $84.75\% \pm 3.16\%$ to $92.59\% \pm 4.78\%$, respectively. This result suggests that the adsorption process in the present work is endothermic (as will be evidenced later in the text). This result corresponds to the fact that the increase in the temperature of the solution promoted the activity of the surface and the kinetic energy of the dye, increasing the diffusion through the film and the pores [30].

3.2.4. Kinetic study

The kinetic models of Lagergren pseudo-second-order, Weber–Morris, and Elovich kinetic, were used to investigate

the mechanism of adsorption of EMHS for aqueous solution of CR. The comparison between the values of the experimental adsorption capacities (q_{exp}) and calculated (q_{cal}) of the kinetic models are shown in Fig. 6a; observing that the calculated values of the adsorption capacity (q_{cal}) in the models used are very close to experimental values (q_{exp}). These results confirmed that the equations of these models apply adequately to the experimental data obtained. On the other hand, the relation between the contact time and the experimental adsorption capacity of EMHS for the CR dye shows a two-stage adsorption curve: (1) there is a slow increase in the adsorption capacity as a function of the contact time and (2) an almost stable adsorption capacity. This behavior is due to the decrease in the number of active adsorption sites caused by its saturation produced by the contact time with the adsorbed contaminant [31]. The results shown in Fig. 5a confirm that the adsorption capacity of the CR dye is limited up to a time of 1,560 min (26 h) since an increase of 2.84 ± 0.25 to $8.27 \pm 0.25 \text{ mg g}^{-1}$ occurred when increasing the contact time from 60 to 1,560 min, respectively. However, after this time, the adsorption of the dye did not present substantial changes reflecting an equilibrium stage and confirming the saturation of the active sites.

3.2.4.1. Lagergren pseudo-second-order model

The pseudo-second-order kinetic model of Lagergren indicates that adsorption followed a cation exchange process

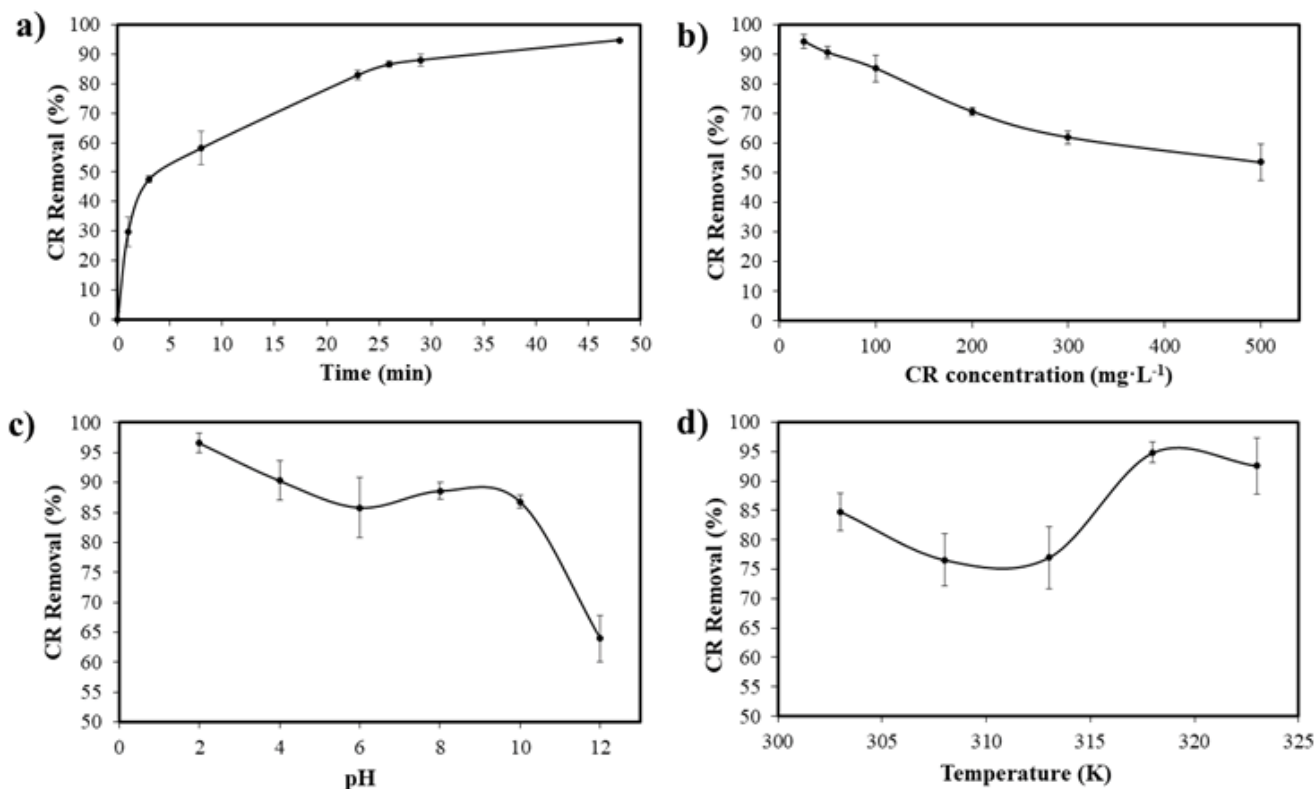


Fig. 5. (a) Removal efficiency of CR dye, (b) effect of the initial concentration, (c) effect of pH and (d) effect of temperature.

between the adsorbent and adsorbate [32]. The kinetic equation of Lagergren is as shown in Eq. (3):

$$\frac{t}{q_t} = \frac{1}{k_2 q_e^2} + \frac{1}{q_e} \quad (3)$$

where q_t is the number of molecules adsorbed at time t (mg g^{-1}) and k is the second-order adsorption rate constant (g (mg min)^{-1}). The parameters of the second-order model were calculated from the slope and intersection when plotting a linear regression of (t/q_t) vs. (t) and are shown in Table 1. The adsorption behavior of the CR dye showed an acceptable correlation with the pseudo-second-order model ($R^2 > 0.99$). The theoretical value obtained from $q_{e,\text{cal}}$ was 9.64 mg g^{-1} ; this result is close to the experimental value of $9.26 \pm 0.18 \text{ mg g}^{-1}$. This similarity between the theoretical and experimental values confirms the correlation between the adsorption results with the kinetic model of pseudo-second-order of Lagergren, suggesting, a chemisorption process between the EMHS and the CR presented in this work. Similar phenomena have been observed for CR adsorption on banana peel dust (0.749 mg g^{-1}) [33], coir pith carbon (6.70 mg g^{-1}) [3], anion exchange membranes (11.01 mg g^{-1}) [34] and anilinepropylsilica xerogel (22.62 mg g^{-1}) [35].

3.2.4.2. Weber–Morris model

The kinetic data obtained in the adsorption were analyzed using the Weber–Morris diffusion model to determine the adsorption mechanism and the control stage. This is an

Table 1

Kinetic parameters for the removal of CR dye using EMHS (298 K, $t = 2,880 \text{ min}$, pH = neutral, $m = 10 \text{ g L}^{-1}$)

Kinetic model	Parameter	Values
Pseudo-second-order	k_2 ($\text{g mg}^{-1} \text{ min}^{-1}$)	4.24×10^{-4}
	$q_{e,\text{cal}}$ (mg g^{-1})	9.64
	R^2	0.995
Weber–Morris	k_{ip} ($\text{mg g}^{-1} \text{ min}^{1/2}$)	0.138
	C	2.409
	R^2	0.956
Elovich	β (g mg^{-1})	0.602
	α ($\text{mg g}^{-1} \text{ min}^{-1}$)	0.137
	R^2	0.987

intra-particle diffusion model used to describe the transport of dissolved molecules from aqueous solutions to the adsorbent material, followed by an intra-particle diffusion/transport process [36]. The model can be expressed with the following equation:

$$q_t = K_{\text{ip}} t^{1/2} + C \quad (4)$$

where k_{ip} is the diffusion rate constant ($\text{mg g}^{-1} \text{ min}^{-1/2}$) and C is the constant (mg g^{-1}) that quantifies the thickness of the boundary layer. The parameters of the model are obtained from the slope and intersection of the graph of q_t vs. $t^{1/2}$.

Table 1 shows these results, which had good correlation with the Weber–Morris model ($R^2 > 0.95$). The absence of an intersection crossing through the origin, suggests that there are different adsorption mechanisms between the CR and the EMHS, including the diffusion of particles.

3.2.4.3. Elovich kinetic model

Elovich kinetic model is used to describe second-order kinetics. This model assumes that the adsorbent surface is energetically heterogeneous and follows a chemical adsorption mechanism. Then, neither desorption nor interactions between the adsorbed species could affect the adsorption kinetics at low superficial coverage [37]. The equation of the Elovich model can be expressed in linear form as:

$$q_t = \frac{1}{\beta} \ln(\alpha\beta) + \frac{1}{\beta} \ln(t) \quad (5)$$

where α is the initial adsorption rate (mg min^{-1}) at the contact time $t = 0$ min and β is the extension of the surface coverage and the activation energy (g mg^{-1}). The constants of the Elovich model, α and β , were calculated with a linear regression of q_t vs. $\ln(t)$, and are reported in Table 1. The adsorption of CR presented good correlation with this model ($R^2 > 0.98$), indicating an energetically heterogeneous behavior of the EMHS in the adsorption of CR.

3.2.5. Adsorption isotherms

The interaction and distribution of contaminant molecules on the surfaces of adsorbents can be understood using isothermal models of adsorption equilibrium. Several models of isotherms have been used for this purpose, such as the model of Langmuir, Freundlich and Temkin. Fig. 6b shows the comparison of the experimental and calculated values of the equilibrium adsorption capacities under different conditions of the isothermal models. The experimental results of adsorption of the CR dye show a continuous increase of the adsorption capacity when increasing the concentration, without reaching a notable adsorption equilibrium, since the absorption capacity increased from 2.33 ± 0.05 to

$25.83 \pm 1.74 \text{ mg g}^{-1}$ with the increase of the initial concentration of 25–500 mg L^{-1} , respectively.

3.2.5.1. Langmuir

The isothermal model of Langmuir is capable of predicting whether the adsorption of molecules takes place on a surface with finite and specific active sites [38]. The linear equation of the Langmuir isotherm model is represented as:

$$\frac{C_e}{q_e} = \frac{1}{bq_{\max}} + \frac{C_e}{q_{\max}} \quad (6)$$

where C_e is the equilibrium concentration of the CR dye in the solution at the end of the adsorption process (mg L^{-1}), q_e is the adsorption capacity of the adsorbent in equilibrium (mg g^{-1}), q_{\max} is the maximum capacity of adsorption of the adsorbent (mg g^{-1}) and b is the Langmuir constant (L mg^{-1}). The parameters of the Langmuir isotherm model are obtained from the regression of C_e/q_e vs. C_e . These values are shown in Table 2. The adsorption of the CR dye exhibited a good fit with the Langmuir isotherm model ($R^2 > 0.95$), so it is possible to affirm that the adsorption of the CR dye assumes

Table 2
Equilibrium isotherm parameters for the removal of CR dye using EMHS (298 K, $t = 2,880$ min, pH = neutral, $m = 10 \text{ g L}^{-1}$)

Isotherm model	Parameter	Values
Langmuir	q_{\max} (mg g^{-1})	153.23
	b (L mg^{-1})	0.005
	R_L	0.241
	R^2	0.956
Freundlich	$1/n$	0.458
	K_F	2.136
	R^2	0.999
Temkin	B_T	4.386
	K_T	0.683
	R^2	0.918

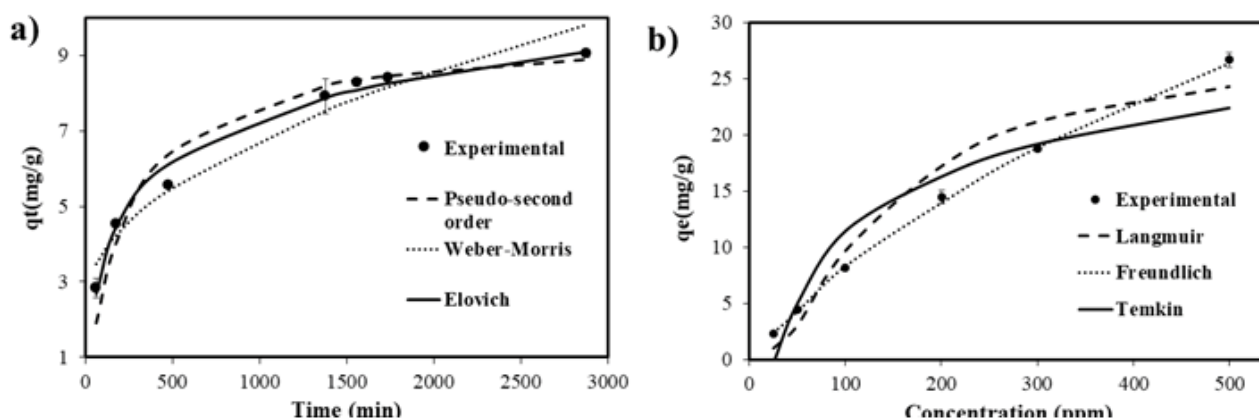


Fig. 6. Kinetic and equilibrium studies of Congo red dye by EMHS; (a) relation between the contact time and adsorption capacity, and (b) effect of the initial concentration on the adsorption capacity.

an adsorption forming a monolayer. From Eq. (6), q_{\max} is 153.23 mg g⁻¹. This value is consistent with the values in the literature where the maximum capacity of adsorption was found to be 1.72 mg g⁻¹ for the adsorption of CR on banana peel dust [33], 16.72 mg g⁻¹ activated carbon containing zinc acetate [39], 40.90 mg g⁻¹ on CaFe₂O₄ magnetic nanoparticles [40], 132.20 mg g⁻¹ sepiolite-poly(dimethylsiloxane) [41], and 151.70 mg g⁻¹ hierarchical NiO nanosheets [42].

The separation factor of the Langmuir isothermal model (R_L), which is used to evaluate when a process of adsorption is favorable ($0 < R_L < 1$), unfavorable ($R_L > 1$) or irreversible ($R_L = 0$), can be calculated by:

$$R_L = \frac{1}{(1 + bC_0)} \quad (7)$$

where b is the Langmuir constant and C_0 is the initial concentration of the dye. Since the value of R_L was 0.24, it reflects a favorable adsorption for the RC dye on the EMHS.

3.2.5.2. Freundlich

The Freundlich isotherm model assumes an adsorption on a heterogeneous surface and multilayer formation, causing a decrease in the binding energy on the surface [43]. The linear equation of Freundlich isothermal model is represented by:

$$\log q_e = \left(\frac{1}{n}\right) \log C_e + \log K_f \quad (8)$$

where K_f and n are the constants of Freundlich in relation to the capacity and intensity of adsorption, respectively. The parameters of the Freundlich isotherm model were calculated from a linear regression of $\log q_e$ vs. $\log C_e$ and are reported in Table 2. The adsorption data of the CR dye showed excellent fit with this model ($R^2 > 0.99$), which states that heterogeneous adsorption and the formation of multiple layers occurs. On the other hand, the value of the heterogeneity factor ($1/n < 1$) indicated that chemical adsorption occurs confirming the above with the Lagergren kinetic model.

3.2.5.3. Temkin

The Temkin model assumes that the adsorption heat of all adsorbate molecules decreases linearly with the adsorbent coverage due to the adsorbent–adsorbate interactions [44,45]. The linear equation of the Temkin isotherm is established by:

$$q_e = B_T \ln K_T + B_T \ln C_e \quad (9)$$

where K_T is the equilibrium constant binding of the isotherm (L g⁻¹), $B_T = RT/b$ is an adsorption heat constant (J mol⁻¹), R is the ideal gas constant (8.314 J mol⁻¹), T is the absolute temperature (K), b is the Temkin constant isotherm.

The parameters of the Temkin isotherm model were obtained from a linear regression of q_e vs. $\ln C_e$ and are presented in Table 2. The adsorption of the CR dye showed a high coefficient of correlation, $R^2 > 0.91$.

Table 3

Thermodynamic parameters for adsorption of Congo red dye on EMHS

Parameter	Temperature	Value
ΔG° (J mol ⁻¹)	303	1,456.88
	308	2,839.09
	313	1,522.35
	318	-1,752.68
	323	53.45
ΔH° (J mol ⁻¹)		46,895.11
ΔS° (J mol ⁻¹ K ⁻¹)		147.12

3.2.6. Thermodynamic study

The thermodynamic parameters, such as Gibbs free energy ΔG° (kJ mol⁻¹), enthalpy ΔH° (kJ mol⁻¹) and entropy ΔS° (kJ mol⁻¹ K⁻¹), for the adsorption of the CR using EMHS can be determined from the temperature dependence, calculated as follows [45]:

$$\ln\left(\frac{q_e}{C_e}\right) = \frac{\Delta S^\circ}{R} - \frac{\Delta H^\circ}{RT} \quad (10)$$

$$\Delta G^\circ = \Delta H^\circ - T\Delta S^\circ \quad (11)$$

where R is the ideal gas constant (8.314 J mol⁻¹ K⁻¹) and T is the absolute temperature (K). The values of ΔH° and ΔS° were calculated from the slope and the intersection of the Van't Hoff plot by linear regression (figure not shown), respectively. Table 3 shows all the thermodynamic parameters. The process of adsorption of CR by EMHS was spontaneous at 318 K, with a negative value of ΔG° (-1,762.68 J mol⁻¹). On the other hand, the positive value of ΔH° (1,358.91 J mol⁻¹) indicates an endothermic adsorption process and chemisorption coinciding with results mentioned in previous sections. Finally, a positive value of ΔS° (147.12 J mol⁻¹ K⁻¹) indicates an increase in the disorder and some structural changes in the surface of the EMHS, as well as during the adsorption of the CR dye.

4. Conclusion

It is evidenced the reuse of EMHS as an adsorbent material in the present work by the removal of anionic dye CR in aqueous solution using batch systems. The physicochemical characterization of the adsorbent showed the formation of the bohemite phase (AlO(OH)) with particle size around 0.40 μm, rough surface, presence of mesopores and high surface area, making the EMHS an excellent candidate for adsorption processes. The adsorption studies were evaluated based on pH, temperature, initial concentration of CR and contact time. A reduction in the percentage of removal of CR by increasing pH or the initial concentration is attributed to the electrostatic repulsion between the OH⁻ and CR on one side and the lack of active sites at high concentrations. However, an opposite effect occurred by increasing the temperature promoted by the thermodynamic characteristics of the process, since the adsorption thermodynamics

exhibited an endothermic and spontaneous process. It is also evidenced the stability of the adsorbent even at different pH values due to the preservation of the crystalline phase at different pH tests. Kinetic calculations indicate that adsorption followed a cation exchange process between the adsorbent and adsorbate according to Lagergren model of pseudo-second-order. Finally, evaluating different adsorption models, the equilibrium results assume an adsorption on a heterogeneous surface and multilayer formation explained by the better correlation with the Freundlich adsorption model. In addition, the maximum retention capacity for this adsorbent is 153.23 mg g⁻¹ that represents an efficient and economical alternative for the removal of organic dyes effluents from wastewater before they are discharged into the water bodies.

Symbols

λ	– Wavelength of the X-rays
B_T	– Adsorption heat constant, J mol ⁻¹
C_0	– Initial concentration of the dye in Langmuir model
C_o	– Final concentration of dye in equilibrium after adsorption
K_F	– Constants of Freundlich in relation to the capacity
K_T	– Equilibrium constant binding of the isotherm, L g ⁻¹
k_{ip}	– Diffusion rate constant, mg g ⁻¹ min ^{-1/2}
q_e	– Absorption capacity of the adsorbent in equilibrium (mg g ⁻¹) in Langmuir model
q_e	– Amount of dye in equilibrium, mg g ⁻¹
q_{max}	– Maximum capacity of adsorption of the adsorbent (mg g ⁻¹) in Langmuir model
q_t	– Number of molecules adsorbed at time t , mg g ⁻¹
ΔG°	– Gibbs free energy
ΔH°	– Heat of adsorption or enthalpy
ΔS°	– Entropy
b	– Temkin constant isotherm
C	– Constant, mg g ⁻¹
C_e	– Equilibrium concentration of the CR dye in the solution at the end of the adsorption process (mg L ⁻¹) in Langmuir model
d_s	– Crystallite size
K	– Constant of Scherrer
k	– Second-order adsorption rate constant, g (mg min) ⁻¹
R	– Ideal gas constant, 8.314 J mol ⁻¹
T	– Absolute temperature, K
β	– Broadening at half of the maximum intensity
θ	– Bragg's angle
V	– Volume of the dye solution, L
b	– Langmuir constant in, L mg ⁻¹
m	– Dry weight of the adsorbent, g
n	– Intensity of adsorption in Freundlich model
α	– Initial adsorption rate (mg min ⁻¹) at the contact time $t = 0$ min in Elovich model
β	– Extension of the surface coverage and the activation energy (g mg ⁻¹) in Elovich model

References

- [1] K. Naseem, Z.H. Farooqi, R. Begum, A. Irfan, Removal of Congo red dye from aqueous medium by its catalytic reduction using sodium borohydride in the presence of various inorganic nano-catalysts: a review, *J. Cleaner Prod.*, 187 (2018) 296–307.
- [2] A. Mittal, J. Mittal, A. Malviya, V.K. Gupta, Adsorptive removal of hazardous anionic dye “Congo red” from wastewater using waste materials and recovery by desorption, *J. Colloid Interface Sci.*, 340 (2009) 16–26.
- [3] C. Namasivayam, D. Kavitha, Removal of Congo Red from water by adsorption onto activated carbon prepared from coir pith, an agricultural solid waste, *Dyes Pigm.*, 54 (2002) 47–58.
- [4] J. Xu, D. Xu, B. Zhu, B. Cheng, C. Jiang, Applied Surface Science Adsorptive removal of an anionic dye Congo red by flower-like hierarchical magnesium oxide (MgO) -graphene oxide composite microspheres, *Appl. Surf. Sci.*, 435 (2018) 1136–1142.
- [5] M. Shaban, M.R. Abukhadra, A. Hamd, R.R. Amin, A. Abdel, Photocatalytic removal of Congo red dye using MCM-48/Ni₂O₃ composite synthesized based on silica gel extracted from rice husk ash ; fabrication and application, *J. Environ. Manage.*, 204 (2017) 189–199.
- [6] G. Zhang, L. Yi, H. Deng, P. Sun, Dyes adsorption using a synthetic carboxymethyl cellulose-acrylic acid adsorbent, *J. Environ. Sci.*, 26 (2014) 1203–1211.
- [7] C. Lei, M. Pi, C. Jiang, B. Cheng, J. Yu, Synthesis of hierarchical porous zinc oxide (ZnO) microspheres with highly efficient adsorption of Congo red, *J. Colloid Interface Sci.*, 490 (2017) 242–251.
- [8] R. Miandad, R. Kumar, M.A. Barakat, C. Basheer, A.S. Aburizaiza, A.S. Nizami, M. Rehan, Untapped conversion of plastic waste char into carbon-metal LDOs for the adsorption of Congo red, *J. Colloid Interface Sci.*, 511 (2018) 402–410.
- [9] M. Hernández-Zamora, E. Cristiani-Urbina, F. Martínez-Jerónimo, H.V. Perales-Vela, T. Ponce-Noyola, M.C. Montes-Horcasitas, R.O. Cañizares-Villanueva, Bioremoval of the azo dye Congo Red by the microalga *Chlorella vulgaris*, 22 (2015) 10811–10823.
- [10] A. Maria, S. Solano, S. Garcia-Segura, C.A. Martínez-Huitle, E. Brillas, Degradation of acidic aqueous solutions of the diazo dye Congo Red by photo-assisted electrochemical processes based on Fenton's reaction chemistry, *Appl. Catal., B*, 168–169 (2015) 559–571.
- [11] S. Li, L. Zhang, J. Wang, B. Wang, Y. Li, C. Ma, Degradation of Congo red induced by air-bubbles in the presence of nanometer TiO₂ powders, *Desal. Wat. Treat.*, 53 (2015) 836–843.
- [12] L. Singh, P. Rekha, S. Chand, Cu-impregnated zeolite Y as highly active and stable heterogeneous Fenton-like catalyst for degradation of Congo red dye, *Sep. Purif. Technol.*, 170 (2016) 321–336.
- [13] D. Malwal, P. Gopinath, Enhanced photocatalytic activity of hierarchical three dimensional metal oxide@CuO nanostructures towards the degradation of Congo red dye under solar radiation, *Catal. Sci. Technol.*, 12 (2016) 4458–4472.
- [14] X. Tian, C. Li, H. Yang, Z. Ye, H. Xu, Spent mushroom: a new low-cost adsorbent for removal of Congo Red from aqueous solutions, *Desal. Wat. Treat.*, 27 (2011) 319–326.
- [15] M.I. Din, Z. Hussain, M.L. Mirza, M.M. Athar, A. Madni, S. Ahmad, Biosorption of toxic congo red dye from aqueous solution by eco-friendly biosorbent *Saccharum bengalense*: kinetics and thermodynamics, *Desal. Wat. Treat.*, 51 (2013) 5638–5648.
- [16] K.G. Bhattacharyya, S.S. Gupta, G.K. Sarma, Kinetics, equilibrium isotherms and thermodynamics of adsorption of Congo red onto natural and acid-treated kaolinite and montmorillonite, *Desal. Wat. Treat.*, 53 (2015) 530–542.
- [17] E.L. Zhang, X.J. Sun, X.T. Liu, Q.D. Wang, Morphology controlled synthesis of α -FeOOH crystals and their shape-dependent adsorption for decontamination of Congo red dye, *Mater. Res. Innovations*, 19 (2015) 385–391.
- [18] L.D. Bortoli, S.M. Palácio, E. Hermes, D.C. Zenatti, M.T. Veit, E.A. Campos, Removal of silver nanoparticles coated with different stabilizers from aqueous medium by electrocoagulation, *Environ. Technol.*, (2019), doi.org/10.1080/09593330.2018.1521877.
- [19] S. Netpradit, P. Thiravetyan, S. Towprayoon, Application of ‘waste’ metal hydroxide sludge for adsorption of azo reactive dyes, *Water Res.*, 37 (2003) 763–772.
- [20] T.M. Adyel, S.H. Rahman, M. Khan, S.M.N. Islam, Analysis of heavy metal in electrocoagulated metal hydroxide sludge

- (EMHS) from the textile industry by energy dispersive X-ray fluorescence (EDXRF), *Metals*, 2 (2012) 478–487.
- [21] L. Luo, W. Cai, J. Zhou, Y. Li, Facile synthesis of boehmite/PVA composite membrane with enhanced adsorption performance towards Cr(VI), *J. Hazard. Mater.*, 318 (2016) 452–459.
- [22] X. Cai, B. Han, S. Deng, Y. Wang, C. Dong, Y. Wang, I. Djerdj, Hydrothermal growth of ZnO nanorods on Zn substrates and their application in degradation of azo dyes under ambient conditions, *Cryst. Eng. Commun.*, 16 (2014) 7761–7770.
- [23] K. Koichumanova, K.B. Sai Sankar Gupta, L. Lefferts, B.L. Mojet, K. Seshan, An *in situ* ATR-IR spectroscopy study of aluminas under aqueous phase reforming conditions, *Phys. Chem. Chem. Phys.*, 17 (2015) 23795–23804.
- [24] M. Hajjami, A. Ghorbani-Choghamarani, R. Ghafouri-Nejad, B. Tahmasbi, Efficient preparation of boehmite silica dopamine sulfamic acid as a novel nanostructured compound and its application as a catalyst in some organic reactions, *New J. Chem.*, 40 (2016) 3066–3074.
- [25] J. Dai, X.H. Liu, Y.J. Xiao, J.H. Yang, P.K. Qi, J. Wang, Y. Wang, Z.W. Zhou, High hydrophilicity and excellent adsorption ability of a stretched polypropylene/graphene oxide composite membrane achieved by plasma assisted surface modification, *RSC Adv.*, 5 (2015) 71240–71252.
- [26] J. Zhang, Z. Yan, J. Ouyang, H. Yang, D. Chen, Highly dispersed sepiolite-based organic modified nanofibers for enhanced adsorption of Congo red, *Appl. Clay Sci.*, 157 (2018) 76–85.
- [27] F. Granados-Correa, J. Jiménez-Becerril, Chromium (VI) adsorption on boehmite, *J. Hazard. Mater.*, 162 (2009) 1178–1184.
- [28] M.T. Yagub, T.K. Sen, S. Afroz, H.M. Ang, Dye and its removal from aqueous solution by adsorption: a review, *Adv. Colloid Interface Sci.*, 209 (2014) 172–84.
- [29] M. Doğan, H. Abak, M. Alkan, Adsorption of methylene blue onto hazelnut shell: kinetics, mechanism and activation parameters, *J. Hazard. Mater.*, 164 (2009) 172–181.
- [30] M.A.M. Salleh, D.K. Mahmoud, W.A.W.A. Karim, A. Idris, Cationic and anionic dye adsorption by agricultural solid wastes: a comprehensive review, *Desalination*, 280 (2011) 1–13.
- [31] Z. Jin, X. Wang, Y. Sun, Y. Ai, X. Wang, Adsorption of 4-*n*-nonylphenol and bisphenol-A on magnetic reduced graphene oxides: a combined experimental and theoretical studies, *Environ. Sci. Technol.*, 49 (2015) 9168–9175.
- [32] J. Fu, Z. Chen, M. Wang, S. Liu, J. Zhang, J. Zhang, R. Han, Q. Xu, Adsorption of methylene blue by a high-efficiency adsorbent (polydopamine microspheres): kinetics, isotherm, thermodynamics and mechanism analysis, *Chem. Eng. J.*, 259 (2015) 53–61.
- [33] N.K. Mondal, S. Kar, Potentiality of banana peel for removal of Congo red dye from aqueous solution: isotherm, kinetics and thermodynamics, *Appl. Water Sci.*, 8 (2018) 157.
- [34] M.I. Khan, S. Akthar, S. Zafar, A. Shaheen, Removal of Congo Red from aqueous solution by anion exchange membrane (EBTAC): adsorption kinetics and thermodynamics, *Materials*, 8 (2015) 4147–4161.
- [35] F.A. Pavan, S.L.P. Dias, E.C. Lima, E.V. Benvenuti, Removal of Congo red from aqueous solution by anilinepropylsilica xerogel, *Dyes Pigm.*, 76 (2008) 64–69.
- [36] S. Dawood, T.K. Sen, Removal of anionic dye Congo red from aqueous solution by raw pine and acid-treated pine cone powder as adsorbent: equilibrium, thermodynamic, kinetics, mechanism and process design, *Water Res.*, 46 (2012) 1933–1946.
- [37] E. Bulut, M. Özacar, I.A. Şengil, Adsorption of malachite green onto bentonite: equilibrium and kinetic studies and process design, *Microporous Mesoporous Mater.*, 115 (2008) 234–246.
- [38] A. Asfaram, M. Ghaedi, A. Goudarzi, M. Rajabi, Response surface methodology approach for optimization of simultaneous dye and metal ion ultrasound-assisted adsorption onto Mn doped Fe₃O₄-NPs loaded on AC: kinetic and isothermal studies, *Dalton Trans.*, 44 (2015) 14707–14723.
- [39] W. Qu, Q. Hu, Y. Zhu, J. Peng, L. Zhang, Microwave-assisted regeneration of spent activated carbon containing zinc acetate and its application for removal of congo red, *Desal. Wat. Treat.*, 57 (2016) 28496–28511.
- [40] X. Liu, S. An, Y. Wang, Q. Yang, L. Zhang, Rapid selective separation and recovery of a specific target dye from mixture consisted of different dyes by magnetic Ca-ferrites nanoparticles, *Chem. Eng. J.*, 262 (2015) 517–526.
- [41] S. Vahidhabanu, A.A. Idowu, D. Karuppasamy, B.R. Babu, M. Vineetha, Microwave initiated facile formation of sepiolite-poly(dimethylsiloxane) nanohybrid for effective removal of congo red dye from aqueous solution, *ACS Sustainable Chem. Eng.*, 5 (2017) 10361–10370.
- [42] B. Cheng, Y. Le, W. Cai, J. Yu, Synthesis of hierarchical Ni(OH)₂ and NiO nanosheets and their adsorption kinetics and isotherms to Congo red in water, *J. Hazard. Mater.*, 185 (2011) 889–897.
- [43] J. Febrianto, A.N. Kosasih, J. Sunarso, Y.H. Ju, N. Indraswati, S. Ismadji, Equilibrium and kinetic studies in adsorption of heavy metals using biosorbent: a summary of recent studies, *J. Hazard. Mater.*, 162 (2009) 616–645.
- [44] I.A.W. Tan, A.L. Ahmad, B.H. Hameed, Adsorption of basic dye on high-surface-area activated carbon prepared from coconut husk: equilibrium, kinetic and thermodynamic studies, *J. Hazard. Mater.*, 154 (2008) 337–346.
- [45] P. Senthil Kumar, S. Ramalingam, C. Senthamarai, M. Niranjana, P. Vijayalakshmi, S. Sivanesan, Adsorption of dye from aqueous solution by cashew nut shell: studies on equilibrium isotherm, kinetics and thermodynamics of interactions, *Desalination*, 261 (2010) 52–60.